

# A Uniform Fault Identification and Location Method of Integrated Energy System

Junjie Zhong<sup>1</sup>, Yong Li<sup>1,\*</sup>, Yijia Cao<sup>1</sup>, Denis Sidorov<sup>2</sup>, Daniil Panasetsky<sup>2</sup>

<sup>1</sup> College of Electrical and Information Engineering, Hunan University, Changsha, China

<sup>2</sup> Energy Systems Institute, Russian Academy of Sciences, Irkutsk, Russia

**Abstract** — With the development of energy coupling devices such as combined cooling/heating and power (CCHP), gas turbines and electricgas transfer device, various energy subsystems are closely coupled into an integrated energy system (IES). Whether it is a power system, a natural gas system or a heating system, a failure in any of them will threaten the safe and reliable operation of the entire IES. Given the lack of unified identification and location of IES faults in existing research, this paper presents a method of unified identification and location of faults using big data analysis. First, the energy hub is used as an energy coupling element, and the dynamic system of natural gas and the model of the regional heating system are established. Combining the analysis of the interaction of other subsystems with other energy systems, the typical features of energy subsystems collected by intelligent terminals are extracted, and the heterogeneous features are spatially and temporally merged into a high dimensional spacetime state detection matrix. The matrix is nonlinearly dimensioned using the Isomap algorithm, and the IES fault identification and location is performed based on the value of the local sparsity coefficient (LSC) value and the node association. The proposed method is validated by the case study.

**Index Terms** — integrated energy system; interaction; fault identification; fault location; big data

## I. INTRODUCTION

With an increase in energy consumption and the distributed generation (DG) accessing to the grid, the limitations of the existing energy system architecture

and the contradiction between supply and demand are highlighted. The Energy Internet (EI) can provide a viable solution [1]. EI transforms or even subverts the existing energy industry, to achieve a decentralized mode of production, and promote the large scale development of renewable energy. Integrated energy system (IES) [2,3,4] is an essential physical carrier of EI [5], including electricity, gas, heat (cold) and other energy sources, which is the key to realize the multienergy complementary and cascade utilization of energy.

The safety and stability of the IES determine the normal operation and function of EI. The subsystems of the IES are tightly coupled, if the power grid fails, the state of the coupling unit (energy hub) will be affected, which will lead to a change in the state of the natural gas network and the heat network [6], and vice versa. Therefore, no matter which subsystem fails, this may lead to cascading failures, affect other energy subsystems, and ultimately threaten the economic and reliable operation of IES. Due to differences in physical characteristics, many sophisticated protection methods in a specific system are challenging to be applied to other subsystems. Furthermore, due to the high degree of coupling among subsystems, it is difficult to unify the identification of faults in the power grid, natural gas or heating system.

The papers [79] put forward several methods of distribution network protection, such as using state estimator based parallel synchronous phasor measurements to detect and identify faults in real time. The failure of natural gas pipelines is identified based on the failure probability index [10]. An artificial intelligence method is proposed to detect the leakage fault of the heat network [11]. In [12], an electric-gas IES model is proposed to assess the impact of natural gas regasification terminals on the electricity and gas sector in Colombia. A framework, consisting of the natural gas transient model and power system steadystate model, is established based on AC optimal power flow [13]. In [14], the interaction between electric and heating based on cogeneration technology is simulated to ensure the safety of energy supply. However, these studies focus either on the single energy subsystem,

\* Corresponding author.

E-mail: [yongli@hnu.edu.cn](mailto:yongli@hnu.edu.cn)

<http://dx.doi.org/10.25729/esr.2018.03.0002>

Received August 21, 2018. Revised November 26, 2018.

Accepted December 19, 2018. Available online January 25, 2019.

© 2018 ESI SB RAS and authors. All rights reserved.

or are limited to the study of interaction among systems.

Considering that the IES has the characteristics of rich data and low-value density [1], it is hard for the traditional protection methods to meet the requirements of IES. In view of this, based on the detailed analysis of the fault characteristics of IES, this paper proposes a big data analysis method based on the Isomap algorithm [15] and the local sparse coefficient (LSC) [16]. The information uploaded by the terminals is used to integrate the multiple subsystem features into a comprehensive feature. Then, the multidimensional matrix is formed by data preprocessing and data aggregation, and the matrix is nonlinearly dimensioned by Isomap. Finally, the LSC value of each node is calculated based on the LSC method, and the fault of IES is located. This method can break the barriers between networks and unify the identification of faults and areas where they occur in power grid, natural gas and heat grid. The proposed method is validated by the case study.

## II. INTEGRATED ENERGY SYSTEM MODELING

### A. Natural Gas Network Modeling

The natural gas network is a typical pipeline network with apparent delay [17]. To improve the accuracy of the simulation results, the dynamic equation is used to describe the gas pipes. The following continuity equation and the motion equation [18] are obtained by:

$$\begin{cases} \frac{\partial(\rho\omega)}{\partial x} + \frac{\partial\rho}{\partial t} = 0 \\ \frac{\partial(\rho\omega)}{\partial t} + \frac{\partial(\rho\omega^2)}{\partial x} + \frac{\partial p}{\partial x} + g(\rho - \rho_a)\sin\alpha + \frac{\lambda}{d} \frac{\omega^2}{2} \rho = 0 \end{cases} \quad (1)$$

where  $\rho$  is the gas density,  $p$  is the absolute pressure,  $\omega$  is the velocity of the pipeline flow,  $x$  and  $t$  are distance and time respectively,  $g$  is gravity acceleration,  $\alpha$  is the angle between pipe and the horizontal line,  $d$  is pipe radius,  $\lambda$  is a coefficient of friction.

The linearized method [19] is adopted to solve the equation. Assuming that the height of the pipeline is unchanged, this means the fourth item in the equation of motion is zero. Furthermore, ignoring the convection item (the second item), this item exists only when the fluid velocity is near the sound velocity. Let  $M$  represent  $A$ , therefore, the equation can be changed into:

$$\frac{\partial M}{A\partial x} + \frac{\partial\rho}{\partial t} = 0 \quad (2)$$

$$\frac{\partial(\rho\omega)}{\partial t} + \frac{\partial p}{\partial x} + \frac{\lambda}{d} \frac{\omega^2}{2} \rho = 0 \quad (3)$$

where  $M$  is the mass flow,  $A$  is the cross-sectional area of the pipe.

To linearize the model, we use the average gas velocity  $\varpi$  [19] to approximate the square item of  $\omega$  in (3):

$$\frac{\lambda}{d} \frac{\omega^2}{2} \rho = \frac{\lambda\varpi}{2d} \rho \quad (1)$$

Substitute (4) into (3):

$$\frac{\partial M}{A\partial t} + \frac{\partial p}{\partial x} + \frac{\lambda}{d} \frac{\varpi}{2A} M = 0 \quad (2)$$

The state equation can link the gas density and pressure. This work adopts a simple relationship (6) between the pressure and density using the sound velocity  $c$

$$p = c^2 \rho \quad (6)$$

Finally, the Wendroff difference method is used [20] to approximate (2) and (5), and get the following equations:

$$\rho_{j,t+1} + \rho_{i,t+1} - \rho_{j,t} - \rho_{i,t} + \frac{\Delta t}{L_{ij}A_{ij}}(M_{j,t+1} - M_{i,t+1} + M_{j,t} - M_{i,t}) = 0 \quad (7)$$

$$\frac{1}{A_{ij}}(M_{j,t+1} + M_{i,t+1} - M_{j,t} - M_{i,t}) + \frac{\Delta t}{L_{ij}}(p_{j,t+1} - p_{i,t+1} + p_{j,t} - p_{i,t}) + \frac{\lambda\varpi_{ij}\Delta t}{4d_{ij}A_{ij}}(M_{j,t+1} + M_{i,t+1} + M_{j,t} + M_{i,t}) = 0 \quad (8)$$

### B. Heat Network Model

In the heat network [21], the hydraulic conditions are used to describe the distribution of flow and pressure, and thermal conditions are used to describe the distribution of temperature and heat supply.

1) Hydraulic Conditions: The resistance loss in the heat network is calculated by

$$\Delta P = \Delta P_f + \Delta P_j \quad (9)$$

$$\Delta P_f = RL \quad (10)$$

$$R = 6.25 \times 10^{-2} \frac{M^2 \lambda_R}{d^5 \rho} \quad (11)$$

$$\lambda_R = 0.11 \times \left(\frac{k}{d}\right)^{0.25} \quad (12)$$

$$\Delta P_j = \alpha RL \quad (13)$$

where  $\Delta P$  is the loss of the pipeline and  $\Delta P_f$  is the loss of resistance along the pipe,  $\Delta P_j$  is the local resistance loss of the pipe,  $\lambda_R$  is the resistance coefficient along the pipeline,  $D$  is the inner diameter of the pipeline,  $\rho$  is the density of fluid,  $k$  is the roughness of the pipeline,  $R$  is the average specific friction of the pipeline,  $L$  is the pipe length,  $\alpha$  is the equivalent coefficient.

The loss of heat dissipation of the pipe is

$$q = \frac{2\pi(t - t_T)}{\frac{1}{\lambda_m} \ln \frac{D_o}{D_i} + \frac{1}{\lambda_T} \ln \frac{4h}{D_i}} \quad (14)$$

where  $t$  is the temperature of the pipeline,  $t_T$  is the temperature of the soil layer,  $\lambda_m$  is the thermal conductivity of the thermal insulation material,  $D_o$  and  $D_i$  are the outer diameter and the inner diameter of the insulation layer of the pipeline, respectively,  $\lambda_T$  is the thermal conductivity of the soil,  $h$  is the buried depth.

The heat loss in one pipeline is converted to mass flow:

$$M_L = 3.6 \times 10^{-3} \frac{qL}{C_p \Delta t} \quad (15)$$

where  $L$  is the pipeline length,  $C_p$  is the specific heat capacity of water,  $\Delta t$  is the temperature difference between the supply and the return water.

2) Thermal Conditions: The relationship between heat power and temperature can be described as:

$$\Phi = C_p M (T_s - T_o) \quad (16)$$

where  $\Phi$  is the thermal load,  $T_s$  is the supply water temperature,  $T_o$  is the return water temperature.

Considering the heat loss of the pipe, its temperature calculation formula is:

$$T_{end} = (T_{start} - T_a) e^{\frac{-\lambda_k L}{C_p M}} + T_a \quad (17)$$

where  $T_{start}$  and  $T_{end}$  represent the water temperature of the incoming and outgoing pipes, and  $T_a$  is the ambient temperature.

At the junction point of the heat network pipe, its temperature is calculated by:

$$(\sum M_{out}) T_{out} = \sum (M_{in} T_{in}) \quad (18)$$

Considering the network topology, and coupling (16) and (17), we can obtain the following correlation equation for the temperature of the supply and return water:

$$C_s (T_s - T_a) = b_s \quad (19)$$

$$C_r (T_r - T_a) = b_r \quad (20)$$

where  $C_s$  and  $C_r$  are the temperature correlation matrix of supply and return water node respectively,  $b_s$  and  $b_r$  are constant vectors.

Heating loads are expressed by

$$Q_l = K_l V_l (T_{in} - T_{out}) \quad (21)$$

where  $K_l$  is the volume index and  $V_l$  is the volume of room.

### C. Energy Hub Modeling

Energy hub [22] is a crucial coupling part of IES, and can be composed of power transformers, microturbine

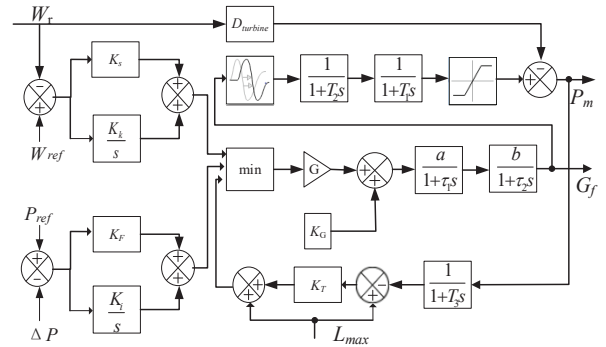


Fig.1. Model of a split shaft gas turbine.

(MT), air conditioners (AC) and heat exchangers (HE). The mathematical model can be expressed as follows:

$$\begin{bmatrix} L_e \\ L_h \end{bmatrix} = \begin{bmatrix} (1 - v_{AC}) \eta^T & \eta_{gc}^{MT} & 0 \\ v_{AC} \eta^{AC} & \eta_{gh}^{MT} & \eta^{HE} \end{bmatrix} \begin{bmatrix} P_e \\ P_g \\ P_h \end{bmatrix} \quad (22)$$

where  $L_e$  and  $L_h$  respectively represent the electrical load and heat load supplied by the energy hub,  $v_{AC}$  is the partition coefficient,  $\eta^T$  is the efficiency of the transformer,  $\eta^{AC}$  is the energy efficiency ratio of AC,  $\eta_{MTgc}$  and  $\eta_{MTgh}$  respectively represent the efficiency of natural gas conversion from MT to electrical and thermal energy,  $\eta^{HE}$  is the efficiency of the HE.  $P_e$ ,  $P_g$  and  $P_h$  are the power, natural gas and heat inputs in the energy hub, respectively.

The gas turbine model uses a split shaft gas turbine [23] and increases the fuel supply system, as shown in Fig.1.

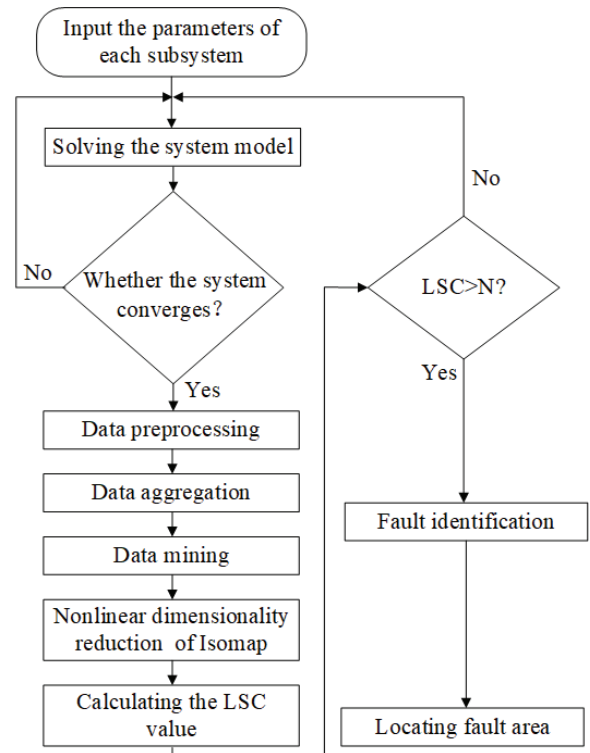


Fig.2. Flowchart of fault location algorithm for IES.

### III. FAULT LOCATION ALGORITHM

#### A. Algorithm Design

The proposed fault location algorithm for IES has the following four parts: data preprocessing, data aggregation, data mining and fault identification. The flowchart is shown in Fig. 2.

#### B. Data Preprocessing

1) Select the Characteristics. According to the difference in fault characteristics of each energy subsystem, three-phase current, negative sequence current, zero sequence current, active power and reactive power are selected as characteristics of power system. The pipe pressure and flow are characteristics of the natural gas system. The heat network flow, supply water pressure, supply water temperature, backwater pressure and backwater temperature are the characteristics of heat network.

2) Construct Network Incidence Matrix. To reflect the topological relationship of IES, the nodes in the system are numbered to determine the area constituted by the nodes and adjacent nodes.

3) Standardize the Data. To eliminate the influence of the dimension and the quantity of the characteristic, the standardization of deviations is used:

$$S_j^i = \frac{S_j^i - \min(S_j)}{\max(S_j) - \min(S_j)} \quad (23)$$

where  $S_j$  represents a dataset and  $S_j^i$  represents a datum in the dataset.

4) Differential Processing. To enhance the difference between the fault node and the normal node, the correlation matrix is used to perform the differential processing of the adjacent nodes and obtain the single-period and single-characteristic matrix  $C_i$ :

$$C_i = |A^T| AT_i \quad (24)$$

where  $A$  is the network incidence matrix; and  $T_i$  is a column matrix formed by the electrical features data.

#### C. Data Aggregation

1) Aggregation in Space. In the space, the single-period and single-characteristic matrix  $C_i$  is expanded into a single period and multi-characteristics matrix  $W_i$ :

$$W_i = [C_1 \ C_2 \ \dots \ C_n] \quad (25)$$

2) Aggregation in Time.  $W_i$  is broadened into a multi-period and multi-characteristics matrix  $W$ .

$$W = [W_1 \ W_2 \ \dots \ W_n] \quad (26)$$

#### D. Data Mining

##### 1) Dimensionality Reduction

Due to the huge amount of data in the high-dimensional matrix  $W$  and the information redundancy of the features, all nodes are clustered together in the high-dimensional manifold, resulting in very little difference. Therefore, it is necessary to reduce dimensionality. Here, the nonlinear

dimensionality reduction using Isomap is introduced [15]. The traditional Euclidean distance matrix is transformed into a geodesic distance matrix, and then the nodes are connected to form the adjacency graph to simulate the real distance of high-dimensional manifold, and effectively reduce the dimension of the manifold. The calculation process is as follows:

1) Build an adjacency graph  $G$ . Based on the Euclidean distance between the adjacent nodes  $i$  and  $j$  of the matrix  $W$ , the nearest  $m$  nodes are selected as the sample nodes for each node. The edge of the graph is introduced to connect the adjacent nodes to construct a weighted graph  $G$  that can represent the adjacent relationship.

2) Calculate the shortest path of any two nodes on the adjacency graph  $G$  to get the geodesic distance matrix  $D$ . Its matrix elements are given by :

$$d_{uv} = \left[ \min_p \sum_{i=1}^{L-1} d^2(p_i, p_{i+1}) \right]^{1/2} \quad (27)$$

where  $p$  is a node sequence of length  $L \geq 2$  and  $p_1 = u$ ,  $p_L = v$ ,  $p_i \in D$ ,  $(p_i, p_{i+1})$  is the nearest neighbor pair of nodes.

3) The centralization matrix  $B$  is calculated by the geodesic distance matrix  $D$ , and its element  $b_{ij}$  is calculated as follows:

$$\begin{cases} a_{ij} = -\frac{1}{2} d_{ij}^2 \\ b_{ij} = a_{ij} - \frac{1}{n} \sum_{j=1}^n a_{ij} - \frac{1}{n} \sum_{i=1}^n a_{ij} + \frac{1}{n^2} \sum_{i=1}^n \sum_{j=1}^n a_{ij} \end{cases} \quad (28)$$

4) Solve the two largest eigenvalues of matrix  $B$  and their corresponding eigenvectors:

$$\lambda_1 \geq \lambda_2 \geq 0 \quad (29)$$

$$x_{(i)}^T x_{(i)} = \lambda_i, 1 \leq i \leq 2 \quad (30)$$

5) Let  $X = [x_{(1)}, x_{(2)}]$  and the matrix  $X$  be the representation of the high-dimensional matrix  $W$  in two-dimensional space after dimension reduction.

##### II) Data Outlier Mining.

After the non-linear dimension reduction of the matrix  $W$ , the distribution of the nodes can be directly reflected. In order to quantitatively analyze the anomaly of the faulty node, the LSC detection of the matrix  $X$  after the dimension reduction needs to be performed. The LSC [16] is an algorithm based on density to detect outliers, which can effectively mine local outliers. The steps are as follows:

1) Find the K-distance ( $K_{\text{dist}}(p)$ ) between each node and its nearest node.

2) Calculate the  $N_{k(p)}$  of each node based on the  $K_{\text{dist}}(p)$ :

$$N_k(p) = \{q \in N / \{p\} | \text{dist}(p, q) \leq K_{\text{dist}}(p)\} \quad (31)$$

where  $\text{dist}(p, q)$  denotes the distance between nodes  $p$  and  $q$ , and this node  $q$  is the nearest neighbor of node  $p$ .

3) Calculate the local sparsity rate of node  $p$ :

$$lsr_k(p) = \frac{|N_{k(p)}|}{\sum_{q \in N_{k(p)}} dis(p, q)} \quad (32)$$

where  $|N_{k(p)}|$  represents the number of nodes in the  $K_{dist}(p)$  of node  $p$ , and  $q$  represents any node in the  $K_{dist}(p)$ . The smaller the local sparsity rate of the node, the greater the possibility of reflecting the node anomaly.

4) In the outlier monitoring, the local sparsity rate of the abnormal nodes should be less than the approximate average of all the nodes. In view of this, a threshold can be set to prune the candidate data sets, thus greatly improving the efficiency of the algorithm and reducing the candidate set. The threshold is called a pruning factor ( $Pf$ ):

$$Pf = \frac{\sum |N_{k(p)}|}{\sum \sum_{q \in N_{k(p)}} dis(p, q)} \quad (33)$$

5) After removing the normal nodes with local sparsity rate greater than or equal to the  $Pf$  from the candidate set, the LSC is used to judge whether the node is abnormal. The LSC value of the node is calculated as follows:

$$LSC_k(p) = \frac{\sum_{q \in N_{k(p)}} \frac{lsr_k(q)}{lsr_k(p)}}{|N_{k(p)}|} \quad (34)$$

### E. Fault Identification

When there is no fault in the IES, all nodes are clustered

together in a high-dimensional manifold without outliers, and the LSC values of all nodes are also approximately equal to 1. When there are faults in the system, some nodes will be far away from other nodes and become outliers, and their LSC values will be much greater than 1. This paper sets the LSC threshold of 3 (the threshold setting is usually adjusted depending on the sample). When the LSC value of the node exceeds the setting value 3, it indicates that the fault occurs in the public area where the nodes with the abnormal LSC value are located.

## IV. CASE STUDY

As shown in Fig. 3, the IES consists of an improved IEEE 14-node power system, a 16-node natural gas system in the Michigan area of the United States [24], an 11-node heat network [25] and an energy hub. In the power system, node 8 is powered by the energy hub, and node 9 provides power to the energy hub. In a natural gas system, node 19 supplies gas to a split shaft gas turbine. Node 36 provides heat to the energy hub.

### I. Interaction Between Faults in an IES

#### 1) Short Circuit Fault of the Power System.

As shown in Fig. 4(a), a single-phase short circuit fault occurred between nodes 4 and 9, resulting in a change in the A-phase current of the line 4-9. In Figs. 4(b) and (c), the flow of natural gas from source nodes 15 and 24 increases correspondingly due to the function of energy hub. The heat network has larger hysteresis of flow and heat transfer. Therefore, the flow rate of heat sink node 31 is affected after a certain time, and the flow rate is slightly higher.

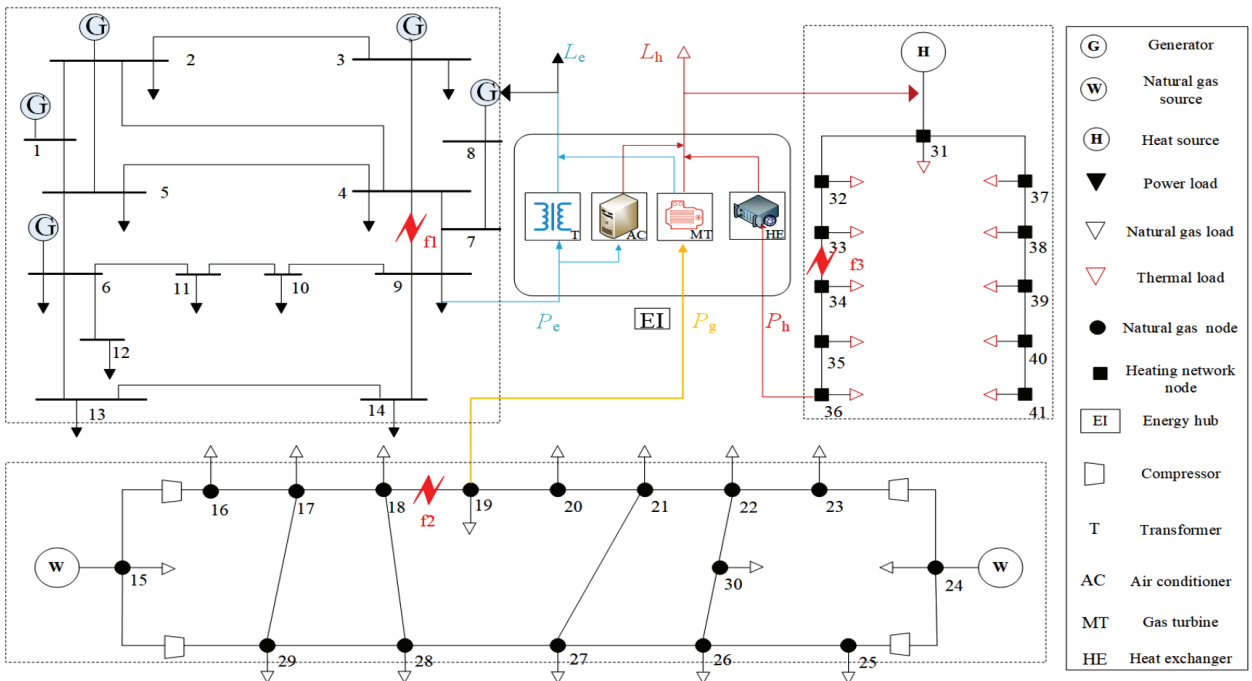


Fig.3. The model of integrated energy system.

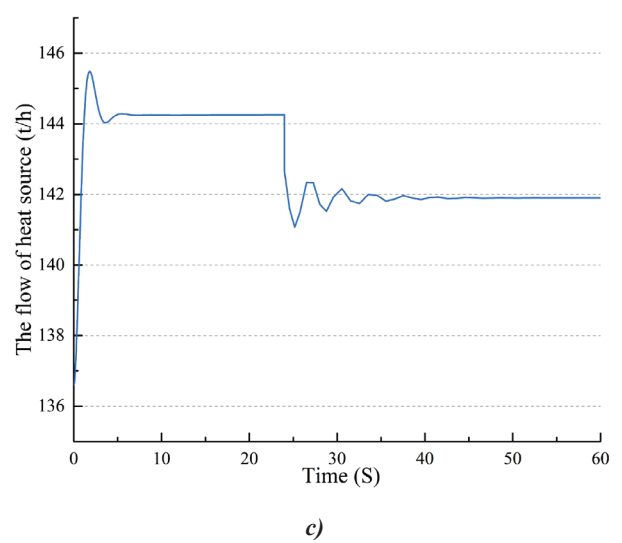
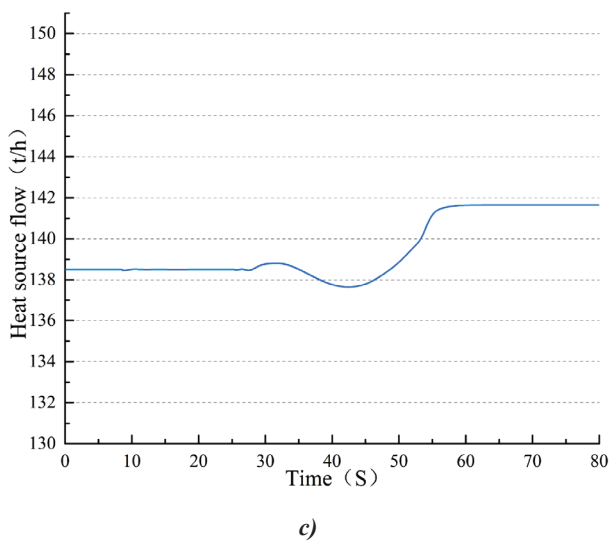
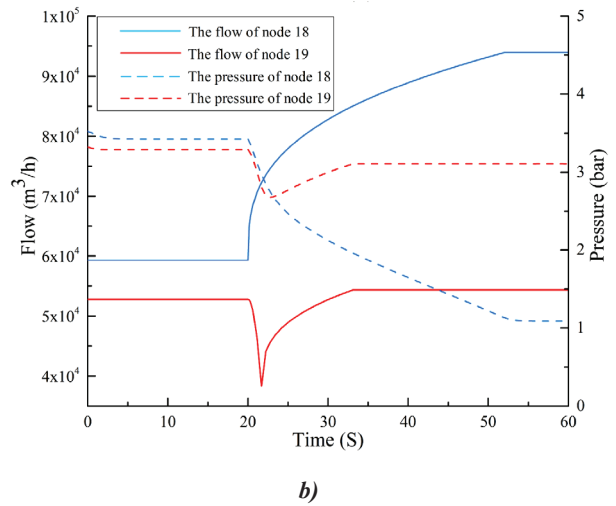
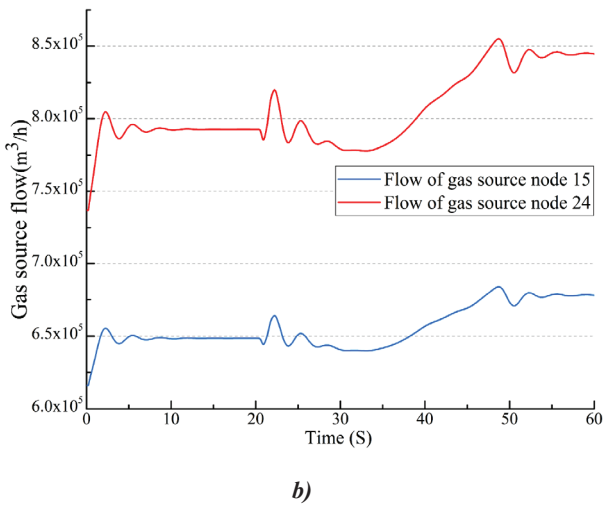
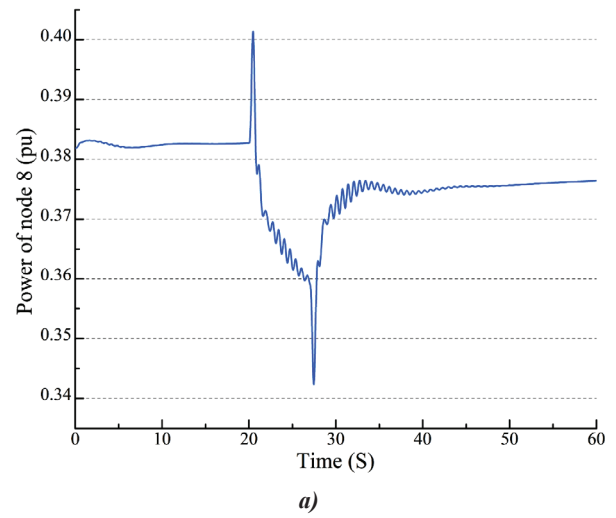
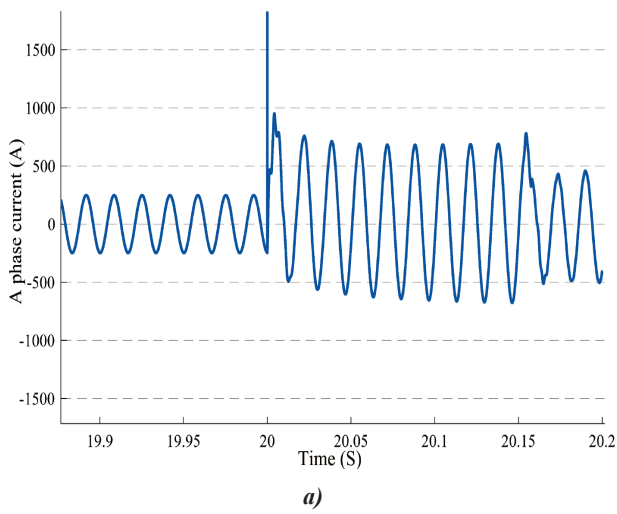


Fig. 4. The typical node waveform for power system fault. (a) A phase current of the line 4-9. (b) Gas source nodes 15 and 24 flows. (c) Heat source node 31 flow.

Fig. 5. The typical node waveform for natural gas system fault. (a) The power of synchronous generator node 8. (b) The pressure and flow of nodes 18 and 19. (c) Heat source node 31 flow.

2) Leakage Fault of the Natural Gas Network.

As shown in Fig. 5(b), a pipeline leak fault f2 occurred between nodes 18 and 19. As the natural gas flows from node 18 to node 19, when the leakage occurs, the leak point pressure gradually decreases, resulting in an increase in the flow from node 18. The pressure of node 18 descends to near the standard atmospheric pressure (101.325kPa). After the fault of node 19, the pressure also goes through a period of decline, but after a certain degree of decline, node 24 will supply node 19 again, due to the dual air source. After the fault, the flow rate slightly increases, while the pressure slightly declines. As shown in Figs. 5(a) and 5 (c), due to the natural gas system failure, node 8 in the power system is restarted after short-term power-off. Node 31 of the heat network characteristic also fluctuates.

3) Water Leakage of the Heat Network.

As shown in Fig. 6(c), a water leakage of 20% occurs in the area f3 between nodes 33 and 34. Due to the reduced resistance, the total heat flow will increase. Except for the constant pressure of node 31, the pressure of other supply and return water nodes decrease (the underlined nodes in the Figure are the return water nodes corresponding to the supply water nodes). The pressure drop of nodes 33 and 34 is the largest, and the farther the distance from the leakage point, the smaller the pressure drop. Compared with the normal condition, the hydraulic gradient of the pipe at the upstream of the fault becomes steeper and the hydraulic gradient of the downstream pipe slows down.

As shown in Figs. 6(a) and (b), the output of the gas turbine also increases due to the increased heat network flow. Therefore, the flow of natural gas source is higher. The active output of node 8 is slightly increased.

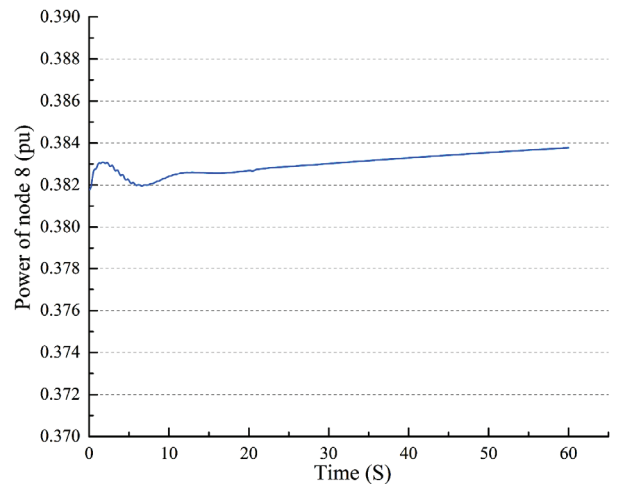
II. Fault Identification Among IES

1) The Fault of Power System.

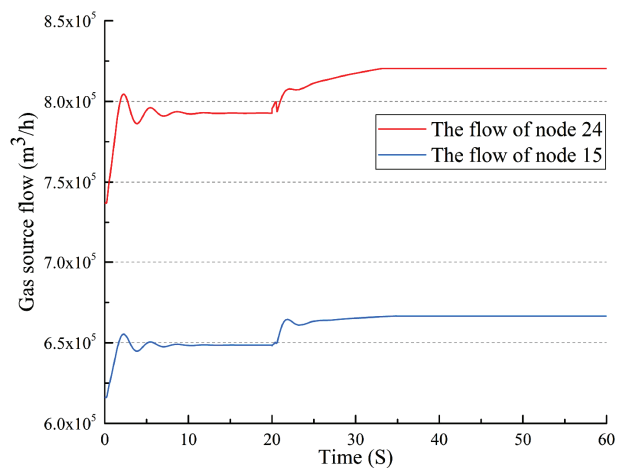
As shown in Fig. 7(a), the Isomap analysis shows that nodes 4 and 9 are distributed to the upper right side of the origin of coordinates, leaving the other nodes as outliers, while other nodes gather near the origin of coordinates. In Fig. 7(b), to reduce the error and increase the fault identification rate, this paper adjusts the  $k$  value of LSC repeatedly to determine the LSC value of nodes (the setting of  $k$  value needs to be adjusted according to the sample). The LSC values of power system nodes 4 and 9 are respectively from 83 to 105 ( $k = 23$  at peak), from 95 to 112 ( $k = 22$  at peak), both far exceed the threshold of 3. However, the LSC values of other nodes are around 1. Therefore, the fault point is in the common area f1 with nodes 4 and 9 that belongs to the power system.

2) The Fault of Natural Gas Network.

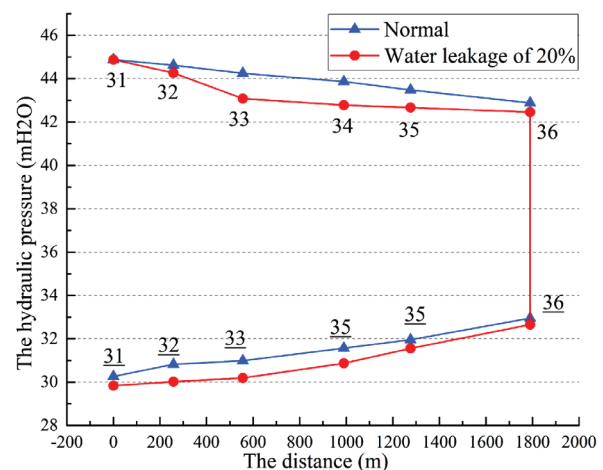
As shown in Fig. 8(a), nodes 18 and 19 of the natural gas system deviate from the origin and become the outliers at the lower rate. Node 8 also deviates slightly, while the other nodes still gather near the origin of coordinates. The



a)



b)



c)

Fig. 6. The typical node waveform for heat network fault. (a) The power of synchronous generator node 8. (b) Gas source nodes 15 and 24 flows. (c) The pressure of the supply and the return water nodes.

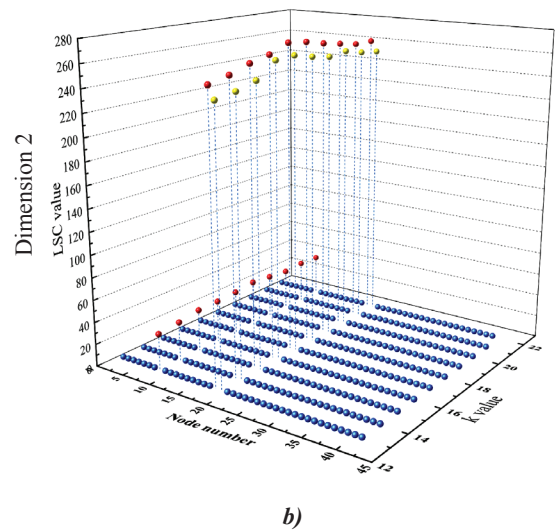
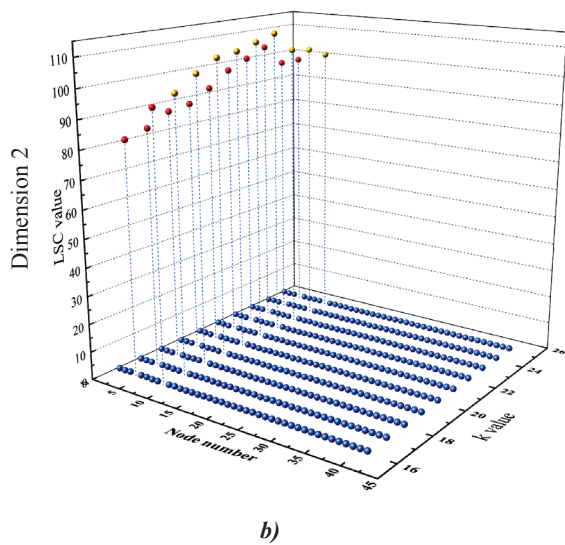
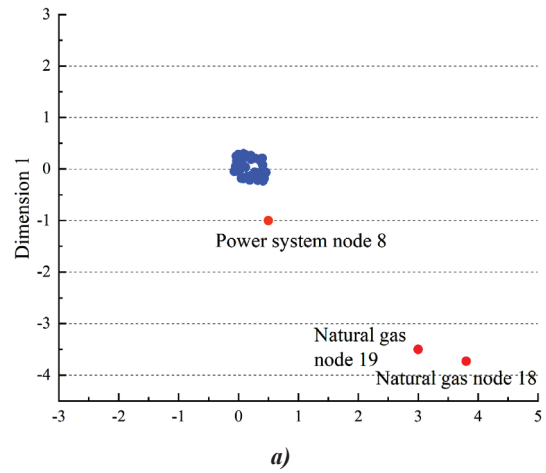
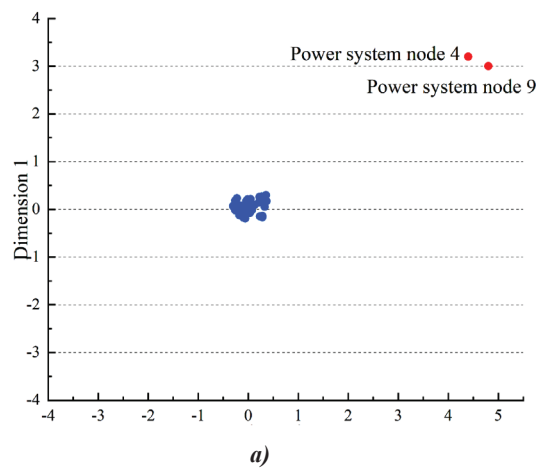


Fig. 7. Fault identification results of the power system fault. (a) Analysis result of the Isomap. (b) Analysis result of LSCat different k values.

Fig. 8. Fault identification results of the natural gas system fault. (a) Analysis result of the Isomap. (b) Analysis result of LSC at different k values.

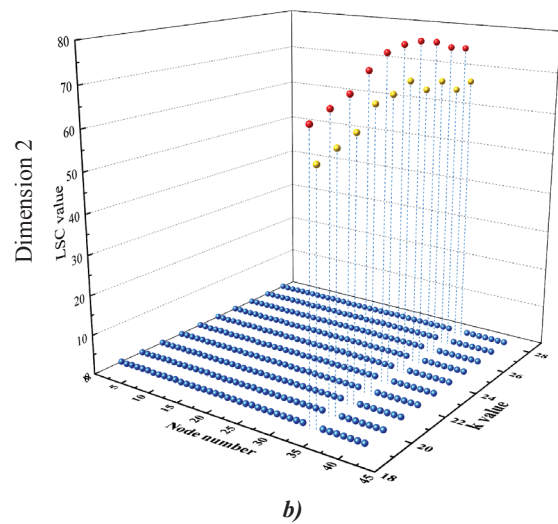
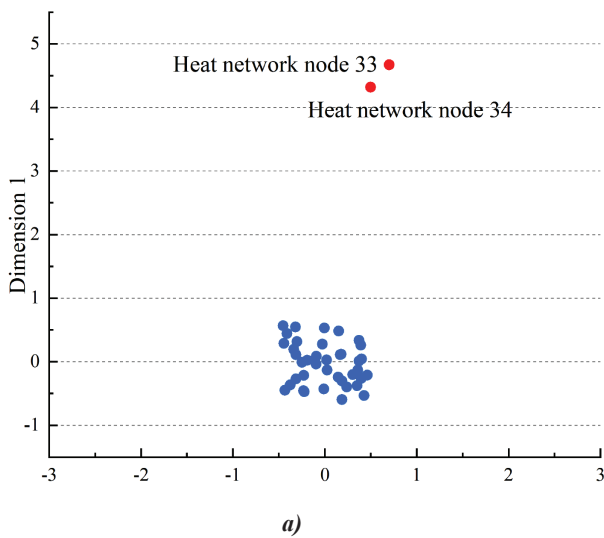


Fig. 9. Fault identification results for the heat network. (a) Analysis result of the Isomap. (b) Analysis result of LSC at different k values.

LSC values of nodes 8, 18 and 19 are from 33 to 41 ( $k=18$  at peak), from 251 to 272 ( $k=18$  at peak), from 240 to 262 ( $k=17$  at peak), respectively. The LSC values of other nodes are all around 1. Node 8 represents an abnormal state of short-time interruption caused by the natural gas system. Combined with the LSC values of nodes 18 and 19, the fault point is in the common area f2 with nodes 18 and 19 that belongs to the natural gas system.

### 3) The Fault of Heat Network.

As shown in Fig. 9(a), nodes 33 and 34 become outliers, while the other nodes are clustered together. The LSC values of nodes 33, 34 are respectively from 67 to 79 ( $k=25$  at peak), from 59 to 71 ( $k=24$  at peak). However, the LSC values of other nodes are around 1. Therefore, the fault point is in the common area f3 with nodes 33 and 34 that belongs to the heat network.

The results of interaction and fault identification in the case studies indicate that the normal nodes converge into clusters, while the abnormal nodes become outliers. Meanwhile, the LSC value of abnormal node is much larger than that of the normal node. According to the above results, when faults occur in different networks, the proposed method can identify the faults of heterogeneous networks belonging to different agents in a unified way, which is conducive and convenient to the improvement of the IES security.

## V. CONCLUSION

This paper proposes a method of state detection and fault location of IES. By combining the characteristics of power, natural gas and heat network, a comprehensive feature quantity is unified, which improves the accuracy of fault identification, and helps to locate the system faults. The interaction caused by a single subsystem after failure is studied, which provides a reference for fault identification and location. Based on the Isomap and LSC methods, the operating data of the IES are used to identify and locate the faults of IES.

This paper considers only one type of faults, therefore the next step of the research will focus on different fault types.

## ACKNOWLEDGEMENT

This work was supported in part by the 111 Project of China under Grant B17016, in part by the Excellent Innovation Youth Program of Changsha of China under Grant KQ1707003, in part by the framework of the research projects III.17.3.1, III.17.4 of the program of fundamental research of the Siberian Branch of Russian Academy of Sciences, reg. No. AAAA-A17-117030310442-8, No. AAAA-A17-117030310438-1. The authors are thankful to the referee for the comments provided.

## REFERENCES

- [1] K. Wang, H. Li, Y. Feng and G. Tian, "Big Data Analytics for System Stability Evaluation Strategy in the Energy Internet," *IEEE Transactions on Industrial Informatics*, vol. 13, no. 4, pp. 1969-1978, Aug. 2017.
- [2] N.I. Voropai, V.A. Stennikov, E.A. Barakhtenko, "Integrated Energy Systems: Challenges, Trends, Philosophy," *Stud. Russ. Econ. Dev.*, vol. 28, no.5, pp. 492-499, 2017.
- [3] N.I. Voropai, V.A. Stennikov, E.A. Barakhtenko, O.N. Voitov, I.V. Postnikov, "A Model for Control of Steady State of Intelligent Integrated Energy System," *Energy Systems Research*, vol. 1, no.1, pp.57-66, 2018.
- [4] N. Voropai, V. Stennikov, S. Senderov, E. Barakhtenko, "Modeling of Integrated Energy Supply Systems: Main Principles, Model, and Applications," *Journal of Energy Engineering*, vol.143, no. 6, Oct. 2017, DOI: 10.1061/(ASCE)EY.1943-7897.0000443
- [5] X. Yu, X. Xu and S. Chen, "A Brief Review to Integrated Energy System and Energy Internet," *Transactions of China Electrotechnical Society*, vol. 31, no. 1, pp. 1-13, March 2016.
- [6] A. A. S. Emhemed, K. Fong, S. Fletcher and G. M. Burt, "Validation of Fast and Selective Protection Scheme for an LVDC Distribution Network," *IEEE Transactions on Power Delivery*, vol. 32, no. 3, pp. 1432-1440, June 2017.
- [7] S. Conti, "Analysis of distribution network protection issues in presence of dispersed generation," *Electric Power Systems Research* 79.1, p.49-56, 2009.
- [8] M. Pignati, L. Zanni, P. Romano, R. Cherkaoui and M. Paolone, "Fault Detection and Faulted Line Identification in Active Distribution Networks Using Synchrophasors-Based Real-Time State Estimation," *IEEE Transactions on Power Delivery*, vol. 32, no. 1, pp. 381-392, Feb. 2017.
- [9] Y. Seyedi and H. Karimi, "Coordinated Protection and Control Based on Synchrophasor Data Processing in Smart Distribution Networks," *IEEE Transactions on Power Systems*, vol. PP, no. 99, pp. 634 - 645.
- [10] G. Dundulis, I. Žutautaitė, R. Janulionis, E. Ušpuras, S. Rimkevičius and M. Eid, "Integrated failure probability estimation based on structural integrity analysis and failure data: Natural gas pipeline case," *Reliability Engineering & System Safety*, vol. 156, pp. 195-202, Dec. 2016
- [11] F. Ren. "Consideration on heat-supply network leakage fault diagnosis," *Shanxi Architecture*, vol.42, no. 28, pp.15-19, Oct. 2016.
- [12] A. Carlos, Saldarriaga-C and S. Harold, Security of the Colombian energy supply: "The need for liquefied natural gas regasification terminals for power and natural gas sectors," *Energy*, vol. 100, no. 1, pp. 349-362, Apr. 2016.
- [13] A. Pambour, C. Erdenerand R. Bolado-Lavin, "Development of a Simulation Framework for

- Analyzing Security of Supply in Integrated Gas and Electric Power Systems,” *Applied Sciences*, vol. 7, no. 1, pp. 47-55, Jun. 2016.
- [14] S. Mashayekh et al., “Security-Constrained Design of Isolated Multi-Energy Microgrids,” *IEEE Transactions on Power Systems*, vol. 33, no. 3, pp. 2452-2462.
- [15] M. Balasubramanian and L. Schwartz, “The Isomap Algorithm and Topological Stability,” *Science*, vol. 7, no. 295, pp. 12-16, Jun. 2002, DOI: 10.1126/science.295.5552.7a.
- [16] X. Weng and J. Shen, “Outlier Mining for Multivariate Time Series Based on Local Sparsity Coefficient,” *World Congress on Intelligent Control & Automation*, vol. 7, pp. 5957 - 5961, Jun. 2006.
- [17] M. Pejovic, M. Pejovic, and R. Maric, “Delay Response of Gas Discharge Tubes,” *Applied Physics Letters*, vol. 60, no. 25, pp. 3188-3190, Jan. 2012.
- [18] D. Jie, X. Diao, et al. “Navier-Stokes simulations of gas flow in micro devices,” *Journal of Micromechanics & Microengineering*, vol. 10, no. 3, pp. 372-380, Dec. 2017.
- [19] X. AI, J. Fang, S. Xu, et al. “An Optimal Energy Flow Model in Integrated Gas-Electric Systems Considering Dynamics of Natural Gas System,” *Power System Technology*, vol. 1535, p. 45-59, 2018.
- [20] T. Wang, Y. Gao, L. Gao, et al. “Time-domain transient response analysis of auto-harness-wire crosstalk based on Implicit Wendroff difference scheme,” *Journal of Jilin University*, vol. 47, no. 2, pp. 392-399, March 2017.
- [21] Wang, Yaran, et al. “Hydraulic performance optimization of meshed district heating network with multiple heat sources,” *Energy*, vol. 126, no. 1, pp. 603-621, May.2017.
- [22] Geidl, Martin, et al. “Energy hubs for the future,” *Power & Energy Magazine IEEE*, vol. 5, no.1, pp. 24-30, 2007.
- [23] Y. El-Sharkh, S. Sisworahardjo and M. Uzunoglu, “Dynamic behavior of PEM fuel cell and microturbine power plants,” *Journal of Power Sources*, vol. 164, no. 1, pp. 315-321, Jan 2007.
- [24] B. Wylie, A. Stoner and L. “Streeter,” “Network: System Transient Calculations by Implicit Method,” *Society of Petroleum Engineers Journal*, vol. 11, no.4, pp. 356-362. Apr.1971.
- [25] L. Liu, et al. “Study on optimal design of urban centralized heat supply pipeline network.” *Shanxi Architecture*, vol. 43, no.32, pp. 24-29. Nov.2017.
- [26] E. Stai, V. Karyotis and S. Papavassiliou, “A hyperbolic space analytics framework for big network data and their applications,” *IEEE Network*, vol. 30, no. 1, pp. 11-17, January-February 2016.
- [27] B. Tang et al., “Incorporating Intelligence in Fog Computing for Big Data Analysis in Smart Cities,” *IEEE Transactions on Industrial Informatics*, vol. 13, no. 5, pp. 2140-2150, Oct. 2017.
- [28] J. Mao, T. Wang, C. Jin and A. Zhou, “Feature Grouping-Based Outlier Detection Upon Streaming Trajectories,” *IEEE Transactions on Knowledge and Data Engineering*, vol. 29, no. 12, pp. 2696-2709, Dec. 1 2017.
- [29] P. Kaur, “Outlier Detection Using Kmeans and Fuzzy Min Max Neural Network in Network Data,” *2016 8th International Conference on Computational Intelligence and Communication Networks (CICN), Tehri*, 2016, pp. 693-696.
- [30] H. Liu, X. Li, J. Li and S. Zhang, “Efficient Outlier Detection for High-Dimensional Data,” *IEEE Transactions on Systems, Man, and Cybernetics: Systems*, no. 48(12), pp. 2451 - 2461, 2017.



**Junjie Zhong** received the BS degree in electrical engineering from Jiangsu University of Science and Technology, Zhenjiang, China, in 2016. He is currently working toward the MS degree from Hunan University, Changsha, China, both in electrical engineering. His research interests are optimization and safety analysis of integrated energy systems.



**Yong Li** (S'09–M'12–SM'14) was born in Henan, Chi-na, in 1982. He received the B.Sc. and Ph.D. degrees in 2004 and 2011, respectively, from the College of Electrical and Information Engineering, Hunan University (HNU), Changsha, China. Since 2009, he worked as a Research Associate at the Institute of Energy Systems, Energy Efficiency, and Energy Economics, TU Dortmund University, Germany, where he received the second Ph. D. degree in June 2012. Since 2014, he is a Full Professor of electrical engineering of HNU. His current research interests include ac/dc energy conversion systems, analysis and control of power quality, and HVDC and FACTS technologies.



**Yijia Cao** (M'98-SM'13) was born in Hunan, China, in 1969. He graduated from Xi'an Jiaotong University, Xi'an, China in 1988 and received M.Sc. degree from Huazhong University of Science and Technology (HUST), Wuhan, China in 1991 and Ph.D from HUST in 1994. Since 2008, he is a full professor and vice president of Hunan University, Changsha, China. His research interests are power system stability control and the application of intelligent systems in power systems.



**Denis Sidorov** (M'08 - SM'18) was born in Irkutsk, Russia, in 1974. He received the Ph.D. and Dr. habil. degrees from Irkutsk State University, Russia, in 1999 and 2014, respectively. Since 2000, he has been a Postdoctoral Research Fellow at Trinity College Dublin and Université de Technologie de Compiègne. He gained his industrial experience in NDT at ASTI Holdings Pte Ltd, Singapore. He was Visiting Professor at Tampere University of Technology, Siegen University. Since 2014, he has been a Leading Researcher at Energy Systems Institute of Russian Academy of Sciences. He serves as IEEE PES Russia (Siberia) Chapter Chair. His research interests include digital signal processing, power quality, interarea oscillations, integral and differential equations theory, machine learning methods, and forecasting. He is the author of more than 170 scientific papers and two monographs.



**Panasetsky Daniil** (S'06-M'13) was born in Bodajbo, Russia in 1983. He received the B.Sc. and Ph.D. degrees in 2006 and 2014, respectively, from Irkutsk State Technical University (ISTU) and Melentiev Energy Systems Institute (MESI), Irkutsk, Russia. Since 2009 he is a senior researcher in MESI. Since 2014 he is an associated professor of electrical engineering in ISTU. His research interests include power system stability, emergency control, ac/dc converters and application of artificial intelligence to power systems.